Nanopaper as an Optical Sensing Platform

Eden Morales-Narváez,[†,#] Hamed Golmohammadi,[†,‡,#] Tina Naghdi,[†,‡] Hossein Yousefi,[§] Uliana Kostiv,[⊥] Daniel Horák,[⊥] Nahid Pourreza,[‡] and Arben Merkoçi*[,†,∥]

[†]ICN2 - Nanobioelectronics & Biosensors Group, Institut Catala de Nanociencia i Nanotecnologia, Campus UAB, Bellaterra, Barcelona 08193, Spain, [‡]Department of Chemistry, College of Science, Shahid Chamran University, Ahvaz 6135743337, Iran, [§]Department of Wood Engineering and Technology, Gorgan University of Agricultural Sciences and Natural Resources, Gorgan 4913815739, Iran, [⊥]Institute of Macromolecular Chemistry, Academy of Sciences of the Czech Republic, Heyrovského Sq. 2, Prague 6 162 06, Czech Republic, and [∥]ICREA - Institucio Catalana de Recerca i Estudis Avançats, Barcelona 08010, Spain. [#]These authors contributed equally to this work.

ABSTRACT Bacterial cellulose nanopaper (BC) is a multifunctional material known for numerous desirable properties: sustainability, biocompatibility, biodegradability, optical transparency, thermal properties, flexibility, high mechanical strength, hydrophilicity, high porosity, broad chemical-modification capabilities and high surface area. Herein, we report various nanopaper-based optical sensing platforms and describe how they can be tuned, using nanomaterials, to exhibit plasmonic or photoluminescent properties that can be exploited for sensing applications. We also describe several nanopaper configurations, including cuvettes, plates and spots that we printed or punched on BC. The platforms include a colorimetric-based sensor based on nanopaper containing embedded silver and gold nanoparticles; a photoluminescent-based sensor, comprising CdSe@ZnS quantum dots conjugated to nanopaper; and a potential up-conversion sensing platform constructed from nanopaper functionalized with $NaYF_4$:Yb^{3+}@Er^{3+}&SiO_2 nanoparticles. We have explored modulation of the plasmonic or photoluminescent properties of these platforms using various model biologically relevant analytes. Moreover, we prove that BC is and advantageous preconcentration platform that facilitates the analysis of small volumes of optically active materials (~4 μL). We are confident that these platforms will pave the way to optical (bio)sensors or theranostic devices that are simple, transparent, flexible, disposable, lightweight, miniaturized and perhaps wearable.

KEYWORDS: nanocellulose · optical sensors · composite · plasmonic devices · photoluminescent devices · biosensing

Owing to its simplicity, natural abundance (*e.g.*, in wood, cotton, hemp and linen) and low cost, cellulose has been widely exploited for myriad purposes, including as an energy source, as a building material, as a textile and for displaying information.[1] Interestingly, cellulose of nanoscale lattice (also known as *nanocellulose*) occurs in diverse morphologies (*e.g.*, nanocrystals, nanofibrils and nanofilms) and exhibits distinctive properties including flexibility, high crystallinity, biodegradability, biocompatibility, optical transparency, hydrophilicity, high porosity, high surface area with hydroxyl-containing groups, and high mechanical strength.[2−4]

As a sustainable material, nanocellulose can be extracted from the disintegration of plant cellulose pulp or synthesized by specific nonpathogenic bacteria: typically, *Acetobacter xylinum* (*A. xylinum*), which are frequently present on naturally grown fruits and in fruit products.[5] In fact, such bacteria produce the chemically purest cellulose films, distinguished by their lack of other plant compounds such as hemicelluloses or lignin.[6] As a tunable material, nanocellulose is being applied and investigated in several fields including biomedicine, energy, textiles and clothing, cosmetics and food products. Particular examples include the low-calorie food "Nata de Coco",[7] wound-healing devices,[8] tissue engineering applications,[9] headphone and loudspeaker membranes,[1] flexible transistors,[10] strain-sensor applications,[11] light-harvesting platforms,[12] solar cells,[13] batteries,[14,15] novel aerogels,[16,17] tools for synthesizing novel nanomaterials,[5] and electrochemical bio/sensing platforms.[18,19]

Paper-based sensors can be advantageous for applications in diagnostics, environmental monitoring and food safety.[20]

* Address correspondence to arben.merkoci@icn.cat.

Received for review April 10, 2015 and accepted July 2, 2015.

Published online July 02, 2015
10.1021/acsnano.5b03097

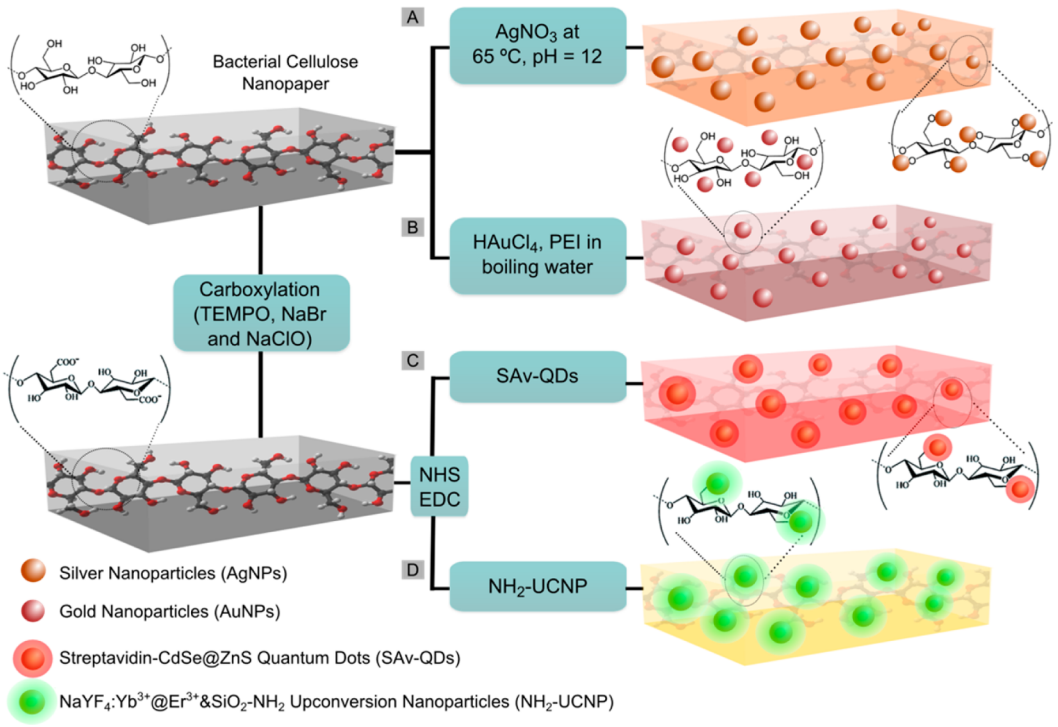

Figure 1. Schematic of the proposed nanopaper-based composites. (A and B) Fabrication of plasmonic nanopaper: (A) silver nanoparticle/bacterial cellulose nanopaper conjugate (AgNP-BC); (B) gold nanoparticle/bacterial cellulose nanopaper conjugate (AuNP-BC). (C and D) Fabrication of photoluminescent nanopaper: (C) streptavidin-coated CdSe@ZnS quantum dot/bacterial cellulose nanopaper conjugate (QD-BC); (D) aminosilica-coated $NaYF_4:Yb^{3+}@Er^{3+}$ up-conversion nanoparticle/bacterial cellulose nanopaper conjugate (UCNP-BC).

Moreover, nanomaterials enable development of miniaturized analytical platforms.[21] However, to date, bacterial nanopaper has been scarcely explored for optical (bio)sensing applications. Hence, we sought to design, fabricate, and test simple, disposable and versatile sensing platforms based on this material.

Herein, we describe various nanopaper-based nanocomposites that exhibit plasmonic or photoluminescent properties that can be modulated using different reagents. We tested different nanopaper configurations, including cuvettes, plates and spots that are printed on nanopaper that contain hydrophobic barriers printed using a wax printer. We evaluated bacterial nanocellulose containing embedded silver nanoparticles (AgNPs) and gold nanoparticles (AuNPs) as a colorimetric-based sensing platform. We also tested a photoluminescent sensing platform based on nanopaper functionalized with CdSe@ZnS quantum dots (QDs) that can be excited *via* UV−visible light. Moreover, we assessed a sensing platform built from nanopaper conjugated to $NaYF_4:Yb^{3+}@Er^{3+}\&SiO_2$ upconversion nanoparticles (UCNPs) that can be excited through infrared light. Lastly, we demonstrate that bacterial cellulose nanopaper (BC) can be exploited as an advantageous preconcentration platform.

RESULTS AND DISCUSSION

The bacterial cellulose employed throughout this research was obtained using a bottom-up approach: the nanofibers were produced by *A. xylinum*, which synthesizes cellulose and subsequently assembles bundles of cellulose nanofibrils.[22] The obtained bacterial cellulose had an average fiber diameter of *ca.* 45 ± 10 nm and an estimated length of greater than 10 μm. This cellulose was characterized using X-ray diffraction to determine its crystallinity (~82%) and crystallite size (~6.3 nm). Moreover, it was assessed for various mechanical parameters: average tensile strength (~345 MPa), Young's modulus (~17.3 GPa) and strain-at-break (~7%). More details on the synthesis and characterization of the bacterial cellulose are provided in the Supporting Information.

The proposed nanopaper-based composites can be obtained using different pathways, which are depicted in Figure 1, including by exploiting the hydroxyl-containing groups of the bacterial cellulose as a reducing agent for chemical reduction of noble metal ions to metal nanoparticles (Route A; see Figure 1A); by adding bacterial cellulose as a nanonetwork to embed metallic nanoparticles during their synthesis (Route B; see Figure 1B); and by producing surface carboxylic groups on the cellulose, for subsequent coupling with protein/amino-functionalized nanoparticles (Route C; Figure 1C,D). The plasmonic nanopaper-based composites AgNP−BC and AuNP−BC were synthesized using Route A and Route B, respectively (see Figures S1 and S2, respectively, in the Supporting Information). The photoluminescent nanopaper-based composites

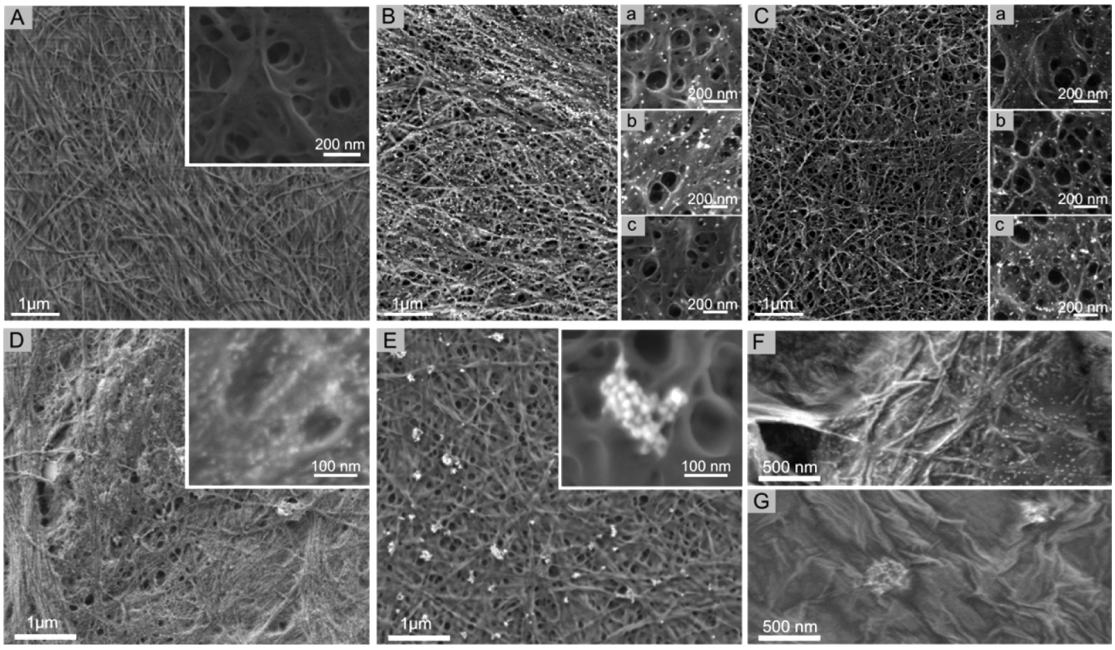

Figure 2. Scanning electron micrographs of the nanopaper-based platforms (performed using carbon conductive tabs as substrate). (A) Scanning electron micrographs of bare bacterial cellulose nanopaper. (B) Scanning electron micrographs of AgNP-BC: (B-a) AgNPs synthesized *in situ* (using bacterial nanopaper as both, a reducing agent and a template); (B-b) AgNP-BC in the presence of 10 μg mL^{-1} of methimazole; (B-c) AgNP-BC in the presence of 4 μg mL^{-1} of iodide. (C) Scanning electron micrographs of AuNP-BC: (C-a) AuNP-BC; (C-b) AuNP-BC in the presence of 8 μg mL^{-1} of thiourea; (C-c) AuNP-BC in the presence of 4 μg mL^{-1} of cyanide. (D) Scanning electron micrographs of QDs embedded within bacterial cellulose nanopaper. (E) Scanning electron micrographs of UCNP-BC. (F) Graphene oxide-coated QD-BC. (G) Graphene oxide-coated UCNP-BC.

QD−BC and UCNP−BC were obtained *via* Route C, as were other composites in which bacterial cellulose was conjugated to aminated nanomaterials (*e.g.*, trypan blue, rhodamine, carbon dots and photoluminescent graphene oxide; see Supporting Information Figure S3).

With the aforementioned nanopaper-based composites in hand, we then delimited or configured them according to shapes or hydrophobic barriers, using punch tools or a wax printing machine, to afford useful devices, including two-dimensional cuvettes, two-dimensional microwell plates, and spots for individual assays (see Supporting Information Figure S4). We reasoned that, owing to their optical transparency, hydrophilicity and chemical-modification capabilities, these bare-cellulose devices could be combined with functional nanomaterials to create sensing platforms. We also envisaged using them as substrates for optical measurements (*e.g.*, absorbance or fluorescence intensity), whereby the analyte would simply be added dropwise onto the bare cellulose. Full details on the overall experimental procedures are provided in the Methods section.

Nanopaper as a Plasmonic Platform. Metal NPs have plasmonic properties: when hit with incident light, their electrons undergo collective motion, which strongly amplifies the local electromagnetic field.[23] In fact, localized surface plasmon resonance of noble metal NPs has been reported to offer potential for sensing applications.[23,24] However, as affirmed in a recent review,[25] there is a lack of suitable building blocks for implementation of plasmonic devices. Given this paucity, we reasoned that our plasmonic nanopaper composites could be easily used as sensing platforms by exploiting analyte−composite interactions that modulate the size, shape, composition, interparticle distance of the NPs, or the refractive index of the surrounding medium. For instance, we envisaged that aggregation or etching of the embedded metal NPs could be exploited for optical sensing.

As representative examples of the potential of functionalized plasmonic nanopaper for optical sensing use, we assessed AgNP−BC as a colorimetric sensor of methimazole or iodide, and AuNP−BC as a colorimetric sensor of thiourea or cyanide. Scanning-electron micrographs of bare BC, AgNP−BC and AuNP−BC are shown in Figure 2A−C, respectively. Nanopaper spots for individual assays were used throughout these experiments (see Figure 3 and Supporting Information Figure S5).

As previously mentioned, we tested our platforms using different biologically relevant compounds: the drug methimazole, the toxic compounds thiourea and cyanide, and iodide. The methimazole can be adsorbed onto AgNPs.[26] As it contains thiol groups, it can act as a linker on AgNPs, thereby promoting their aggregation. This phenomenon can be observed in the AgNP−BC composite shown in Figure 2B-b. Supporting Information Figure S5a illustrates the change in color of AgNP−BC from yellow to dark yellow upon addition of different doses of methimazole (approximately a

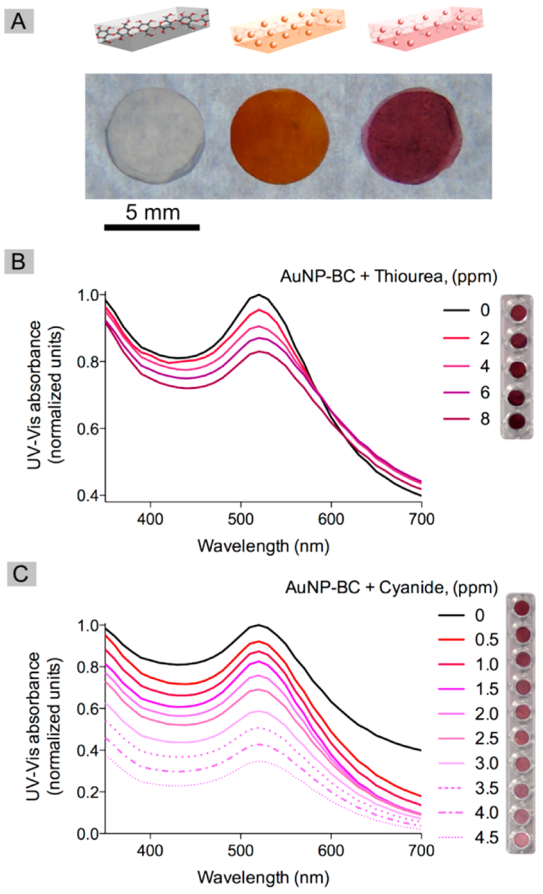

Figure 3. (A) Plasmonic nanopaper spots for individual assays. From left to right: BC, AgNP-BC, and AuNP-BC. (B) Change in color of AuNP-BC upon addition of thiourea. (C) Change in color of AuNP-BC upon addition of cyanide.

few ppm), revealing a slight red-shift in the UV−vis absorption spectrum (see Supporting Information Figure S5a). After 10 ppm methimazole, no color change was observed indicating the saturation of the sensing response. The toxic and hazardous compound thiourea[27] can similarly facilitate the aggregation of AuNPs. Figure 2C-b shows how thiourea affects the AuNP−BC composite at the nanoscale. Figure 3B reveals that the AuNP−BC changes from red to dark red upon addition of thiourea (concentration: roughly a few ppm). A red-shift in the UV−vis absorption spectrum of the AuNP−BC was observed, particularly in the local minimum of the spectra between 350 and 520, (*i.e.*, from 430 to 440 nm), and the sensing response was saturated at 8 ppm thiourea.

Iodide has been reported to etch metal NPs.[28] The effect of iodide on our AgNP−BC composite can be observed in Figure 2B-c: on the basis of our findings, iodide apparently causes the AgNPs appear to shrink, thereby causing their color to change from yellow to light yellow, which is accompanied by blue-shift in the UV−vis spectrum that depends on its concentration (see Supporting Information Figure S5a), showing a saturation from 4 ppm iodide. We observed that cyanide similarly affects the AuNPs embedded in the composite (see Figure 2C-c). Figure 3C shows a change in color, from red to light pink, and the corresponding blue shift in UV−vis absorbance intensity of the AuNP−BC composite upon addition of cyanide (concentration: roughly a few ppm, no color change was observed after 4.5 ppm cyanide). Detailed pictures of the plasmonic nanopaper color change are included in Supporting Information Figure S5a,b. The size-distribution of the aforementioned NPs was roughly estimated by SEM image processing and the results confirmed the overall trend of these phenomena (see Supporting Information Figure S5c,d). The respective calibration curves for these experiments (AgNPs-BC plus methimazole or iodide and AuNPs-BC plus thiourea or cyanide) are shown in Supporting Information Figure S6.

To assess the selectivity of the developed AuNP-BC platform, standard solutions of thiourea (4 ppm) and cyanide (2 ppm) were independently analyzed in the presence of several other ions that are likely to exist in complex matrixes such as water samples. Any relative error equal or greater than ±5% from the analytical signal value was considered as interference. Supporting Information Figure S7 shows that AuNP-BC bears selectivity toward thiourea and cyanide as sensing platform, respectively. Citrate ion did not interfere even at 50 ppm; therefore, it can be applied as a masking agent for 10 ppm of Fe^{3+}, Cu^{2+} and Zn^{2+} for thiourea sensing.

Nanopaper as a Photoluminescent Platform. Quantum dots are semiconductor nanocrystals that exhibit distinctive photophysical properties such as size-tunable emission, narrow and symmetric photoluminescence, broad and strong excitation spectra, strong luminescence and robust photostability.[29] They are generally excited with UV−vis light (*i.e.*, light of wavelength from 320 to 630 nm) to produce Stokes-shifted emission. Quantum dots have been widely employed in diverse applications, including imaging and labeling, in which they act as optical sensing agents.[30,31] Following surface modification of QDs with specific ligands or biomolecules, their photoluminescence can be exploited for signal transduction to report their interaction with a given analyte, which occurs mainly by energy transfer between the QDs and the donor/acceptor molecules.[24,32]

Up-conversion luminescence occurs when multiple low-energy photons (generally in the infrared region) are absorbed by rare-earth lanthanides embedded in a suitable inorganic structure to trigger higher energy (anti-Stokes) luminescence (in the visible region). Interestingly, up-conversion NPs can be excited through near-infrared (700−1100 nm) light, which is the "optical transparency window" of biological tissue to yield visible emission (*e.g.*, blue, green or red). Furthermore, they exhibit robust photostability and high resistance

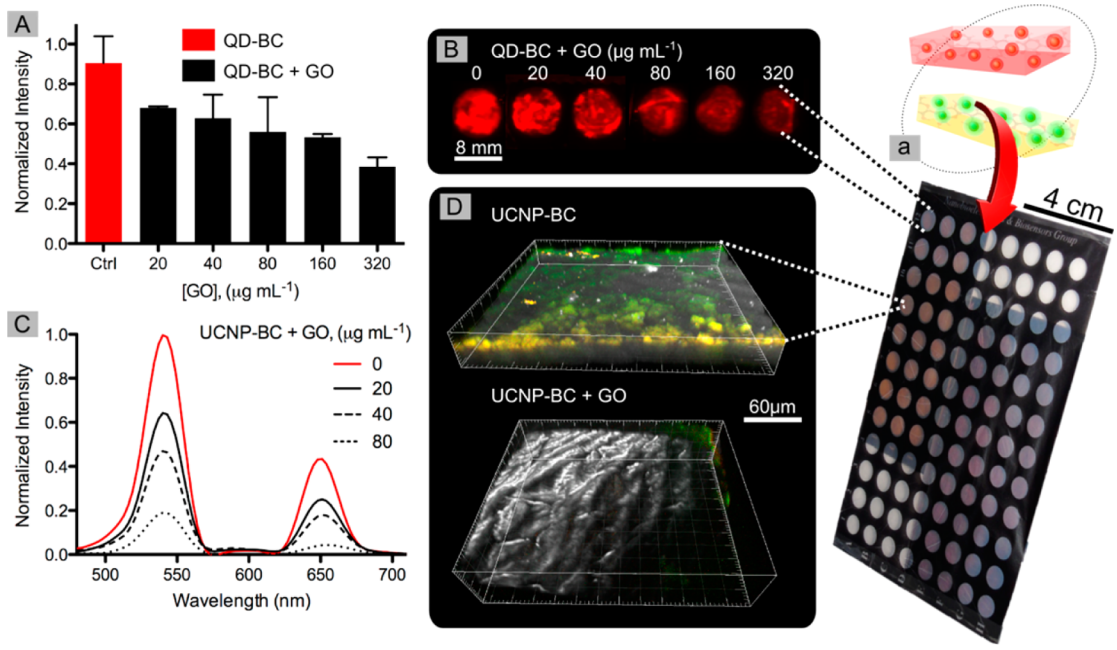

Figure 4. (a) Photoluminescent nanopaper multiwell plate. (A) Modulation of the photoluminescence intensity of QD-BC by addition of graphene oxide at different concentrations. (B) Image of QD-BC wells acquired using a fluorescence scanner. (C) Modulation of the photoluminescence intensity of UCNP-BC by addition of graphene oxide (GO). (D) Confocal microscopy images of UCNP-BC (top) and GO-coated UCNP-BC (bottom).

to photobleaching. Consequently, lanthanide-doped up-conversion NPs are an emerging generation of nanomaterials enabling novel theranostic applications that involve therapy, drug delivery, imaging and sensing. Up-conversion NPs can also be functionalized with specific ligands, biomolecules, dyes or quenchers in order to exploit their interaction with an analyte that modulates the photoluminescence intensity, generally by energy transfer.[33]

Owing to their virtually universal, long-range and highly efficient photoluminescence quenching capabilities, graphene-based materials are being intensely assessed for sensing applications based on energy transfer.[34,35] In the present work, as an experimental example of such energy-transfer, we modulated the photoluminescence of the composites QD-BC and UCNP-BC, using graphene oxide (GO) as an acceptor and either composite as donor, in nanopaper microwell plates prepared as described above (see Figure 4a and Supporting Information Figure S4).

Streptavidin-coated CdSe@ZnS QDs (average size, ~14 nm; maximum emission wavelength, *ca.* 665 nm) were acquired from Life Technologies (New York). Amino-functionalized $NaYF_4$:Yb^{3+}@Er^{3+}&SiO_2 UCNPs with an average size of ~34 nm and two emission peaks at ~550 and ~610 nm, respectively, were synthesized and characterized using TEM, dynamic light scattering and Fourier transform infrared spectroscopy, as described in Supporting Information. Scanning electron micrographs of the QD-BC and the UCNP-BC are shown in Figure 2, panels D and E, respectively. Single-layer GO microsheets (lateral dimensions, 0.18−1.2 μm; C/O ratio, *ca.* 1:1 [manufacturer's data, approximate values]; Angstron Materials Inc., OH) were employed throughout these experiments. Figure 4A,B shows modulation of the QD-BC photoluminescence intensity upon addition of GO at different concentrations (from 20 to 320 μg mL^{-1}). As illustrated in Figure 4B, images of the photoluminescence from the QD-BC microwells were obtained using a fluorescence scanner (excitation wavelength, 488 nm; emission wavelength, 665 nm; laser power, 20 mW at 100%; and PMT, 50%). The scanning electron micrograph in Figure 2F reveals that the QD-BC composite was coated with GO platelets. Moreover, Figure 4C shows modulation of the intensity of the UCNP-BC photoluminescence upon addition of graphene oxide at different concentrations (from 20 to 80 μg mL^{-1}). Figure 4D contains confocal microscopy images of bare UCNP-BC and GO-coated UCNP-BC (excitation wavelength, 980 nm; laser power, 827 mW at 12.5%), and Figure 2G shows a scanning electron micrograph of the GO-coated UCNP-BC. As we expected, these photoluminescent composites were effectively quenched using GO.

Specific ligands or biomolecules such as antibodies and DNA are generally the cornerstone of selectivity and specificity in chemo/biosensing. Taking advantage of the versatility of the developed hybrid materials and aiming at proving that the proposed nanopaer-based composites are amenable to selectivity and specificity, we have exploited GO as a pathogen-revealing agent and antibody decorated QD-BC as a biosensing platform. In other words, a substrate containing antibody

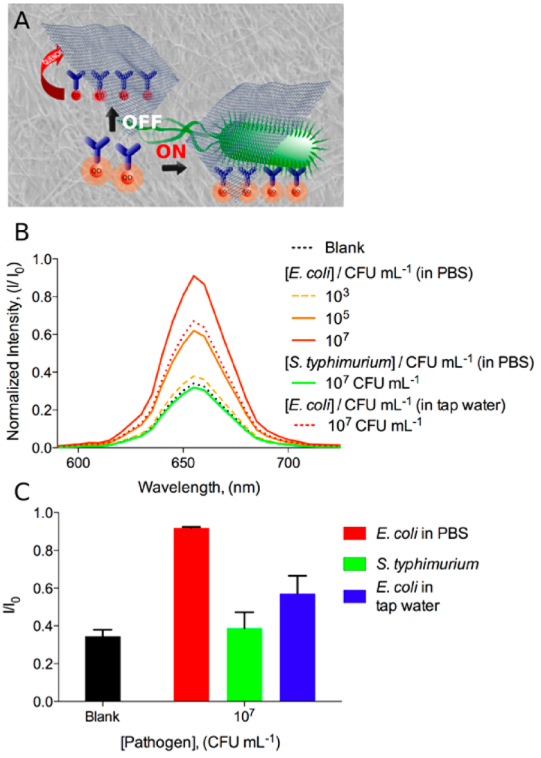

Figure 5. Graphene oxide as a pathogen-revealing agent and antibody decorated QD-BC as a biosensing platform. (A) Schematic representation of the biosensing platform. (B) Spectra of spots for individual assays made of QD-BC (excitation wavelength 480 nm). The spectra display the photoluminescence quenching levels upon GO addition according to the analyzed sample. (C) Photoluminescence quenching levels at the maximum emission wavelength of QD-BC (655 nm) upon GO addition according to the analyzed sample. I/I_0: final photoluminescent intensity divided by starting photoluminescent intensity. Experimental details described in the Methods section.

decorated QDs operates as a photoexcited donor of fluorescence resonance energy transfer (FRET), whereas GO is exploited as FRET acceptor. Such a FRET phenomenon is not observable if the distance between QDs and GO is greater than ~30 nm. Consequently, if a big-sized analyte (such as a pathogen) is captured by the antibody-decorated QDs, the energy of the QDs donors is not transferred after adding the GO acceptor (GO is able to interact with both, the QDs donors and the pathogen by electrostatic interactions). However, FRET is observable in the absence of the pathogen, since GO interacts with the antibody-decorated QDs donors. Hence, the QDs bear a strong photoluminescent emission in the presence of the pathogen, whereas in the absence of the pathogen the QDs are quenched (see Figure 5A). Full details on the operational concept of GO as a pathogen-revealing agent has been previously reported by our research group.[36] Herein, spots for individual assays made of QD-BC were functionalized with biotinylated antibodies against *Escherichia coli* (*E. coli*) through streptavidin–biotin affinity (as mentioned above, the utilized QDs are coated with streptavidin). Phosphate-buffered saline (PBS) and tap water were used as matrixes to perform this novel immunoassay. Blank solutions of these matrixes showed similar photoluminescence quenching levels after adding GO. Figure 5B,C displays: (i) how the intensity of the studied QD-BC spots is quenched in the absence of the target pathogen, whereas the explored QD-BC spots are scarcely quenched upon addition of *E. coli* concentrated at 10^7 CFU mL^{-1}; (ii) that the biofunctionalized QD-BC spots are also quenched upon addition of a high concentration (10^7 CFU mL^{-1}) of a nontarget pathogen such as *Salmonella typhimurium* (*S. typhimurium*), which demonstrates the selectivity and specificity of the biosensing platform; (iii) last, that the explored biosensing platform is able to operate even in a complex matrix such as tap water, since the analysis of a blank solution showed a ~34% of quenching, whereas the analysis of *E. coli* suspended in tap water (at 10^7 CFU mL^{-1}) displayed a ~57% of quenching.

Nanopaper as a Preconcentration Platform. Due to the nanostructure of BC, the spatial distribution of nanoparticles deposited within BC is completely different when compared with the disposition of nanoparticles embedded within other conventional paper substrates such as nitro/cellulose, see Supporting Information Figure S8. In addition, due to the optical transparency of BC, we expected the performance of optically active nanoparticles embedded within BC to be advantageous when compared with other substrate which is commonly utilized in paper-based sensors such as nitrocellulose. In fact, we discovered that the signal intensity of AuNP drop casted on BC outperforms the signal intensity provided by AuNP drop casted on nitrocellulose (at the same concentration). Figure 6A shows the colorimetric profile of different spots, made of bare BC and nitrocellulose, drop casted with AuNP (at two concentration levels: 0.27 and 1.38 μM, respectively). Interestingly, the signal of AuNP measured on BC provided an approximate 2.4-fold enhancement in terms of intensity when compared with the intensity of AuNP measured on nitrocellulose. This result suggests that, owing to its structure, BC operates as a preconcentration membrane, allowing optical properties of the embedded nanoparticles to be virtually completely exposed due to its transparency. This find may open the way to development of novel and advantageous tests based on nanopaper.

Bearing in mind such a preconcentration performance, we also discovered that BC enables measuring the content of small volumes of optically active nanomaterials such as AuNPs and QDs advantageously. Figure 6B displays the photoluminescent spectra of a BC spot drop casted with 4 μL of QDs and the spectra of 4 μL of a QDs colloidal suspension measured on a black microwell plate, respectively (QDs were concentrated at 100 nM, an excitation wavelength of 450 nm was employed). With the use of BC as a support, the QDs

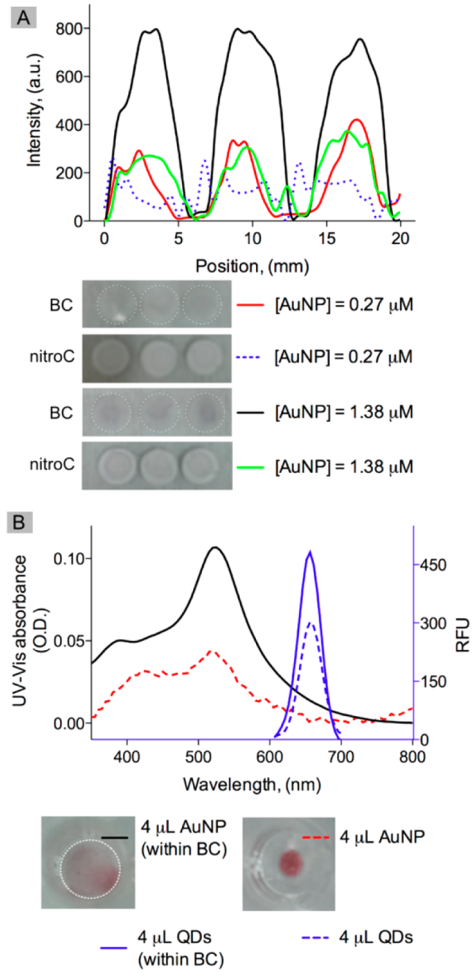

Figure 6. Nanopaper as a preconcentration platform. (A) Colorimetric profile and pictures of AuNP deposited on bacterial cellulose nanopaper (BC) and nitrocellulose (nitroC). (B) UV−vis/photoluminescent spectra of 4 μL of [AuNP] = 1.84 μM and 4 μL of [QDs] = 100 nM obtained on BC and microwells, respectively. QDs were excited at 480 nm.

gave a signal 1.6-fold higher than that of the QDs small drop measured on a microwell. Consequently, BC is likely to preconcentrate and homogenize the content of the small volume of the drop casted sample. Figure 6B also shows the UV−vis spectrum of a BC spot drop casted with 4 μL of AuNPs (concentrated at 1.84 μM), whereas a 4 μL AuNPs drop provided a lower optical density and a noisy spectra using a conventional microwell plate as substrate. This discovery might bring advantages in optical analytical applications where the sample volume to be analyzed is very limited or could be conveniently reduced, for instance, in cerebrospinal fluid analysis, toxicity analysis or samples-containing antibodies or other expensive reagents.

CONCLUSIONS

We have exploited the impressive properties of BC nanopaper to fabricate simple, versatile and disposable platforms for optical sensing. We readily prepared two types of plasmonic nanopaper (AgNP-BC and AuNP-BC) and two types of photoluminescent nanopaper (UCNP-BC and QD-BC) using different nanomaterials, by either using BC as a reducing agent, using it as a template or functionalizing it. In all of these approaches, we took advantage of the optical transparency, porosity, hydrophilicity, and amenability to chemical modification, of BC. We have also shown that BC can be easily turned into useful devices (*e.g.*, cuvettes, multiwell plates and spots) for individual assays by wax printing or by using simple punch tools. We have also demonstrated that the plasmonic or photoluminescent properties of these nanopaper-based composites can be effectively modulated to perform analytical tasks. Additionally, we have proved that the developed platforms are amenable to high selectivity and specificity *via* functionalization with biomolecules such as antibodies and they may operate in complex matrixes. Finally, we discovered that BC can also be exploited as an advantageous preconcentration platform of small volumes of optically active nanomaterials. We believe that this class of platforms will prove valuable for displaying analytical information in diverse fields such as diagnostics, environmental monitoring and food safety. Interestingly, since bacterial cellulose is flexible, lightweight, biocompatible and biodegradable, the proposed composites could be used as wearable optical sensors and could even be integrated into novel theranostic devices.

METHODS

Reagents and Equipment. Trypan blue, rhodamine, NaOH, poly(ethylenimine), $AgNO_3$, $HAuCl_4$, 2,2,6,6-tetramethylpiperidine-1-oxyl (TEMPO), 1-ethyl-3-(3-(dimethylamino)propyl)carbodiimide (EDC), *N*-hydroxysuccinimide (NHS), NaOCl, NaBr, ethanol, phosphate buffered saline tablets, Tween 20, bovine serum albumin, and micowell plates were acquired from Sigma-Aldrich (Taufkirchen, Germany). CdSe@ZnS Streptavidin-QDs 655 were purchased from Life Technologies (Grand Island, New York). Biotinylated antibody against *E. coli* were acquired from Abcam (Cambridge, U.K.). Graphene oxide dispersion was obtained from Angstron Materials, Inc. (Dayton, OH). Cellulose membrane CFSP001700 and nitrocellulose membrane SHF1800425 were acquired from Millipore (Billerica, MA). Particle size distributions were estimated using ImageJ 1.48v (Wayne Rasband, National Institutes of Health, Bethesda, MD). Hydrophobic patterns were printed using a Color Qube 8570 wax printer (Xerox, Wethersfield, CT). UV−vis absorbance and photoluminescence measurements were carried out using a SpectraMax M2e spectrophotometer (Molecular Devices, Sunnyvale, CA). SEM imaging was performed through a Magellan 400L SEM High Resolution SEM (FEI, Hillsboro, OR). EDX analysis was carried out using a Quanta 650F Environmental SEM (FEI, Hillsboro, OR). Photoluminescence images were obtained using a Typhoon 9410 Variable Mode Imager (GE, Freiburg, Germany). Confocal imaging and UCNPs spectra acquisition was performed using a SP5 confocal microscope (Leica, Wetzlar, Germany). Colorimetric profiles were obtained using an ESEQuant Lateral Flow reader (Qiagen, Stockach, Germany).

Bacterial Cellulose Nanopaper (BC) as Reducing Agent for *in Situ* Synthesis of AgNPs. The procedure for *in situ* synthesis of AgNPs within BC was performed according to the following method: the as-received wet BC (15 × 10 × 0.5 cm^3) was soaked in 300 mL double-distilled water, and its pH was adjusted to 12 by 2 M NaOH solution. The reaction mixture was then heated at constant temperature 65 °C for 30 min followed by stirring. Afterward, 75 mL of 0.1% (w/v) $AgNO_3$ solution was gently (about 10 mL/min) added into the reaction mixture. The contents were then kept under continuous heating at 65 °C for 2 h. During the fabrication procedure, the color of BC was first changed from colorless to yellow and then yellow to amber, which indicates the synthesis of silver nanoparticles (AgNPs) according to gradual reduction of silver ions. The contents were then cooled to room temperature and the fabricated AgNP-BC (*in situ* generated AgNPs in BC) was separated from the mixture solution and washed several times with double-distilled water in order to remove any unreacted silver cations or free and loosely attached AgNPs. The fabricated AgNP-BC was stored in dark conditions at 4 °C before being used. The fabrication of AgNP-BC was also confirmed by UV−visible absorption spectra, EDX and SEM analysis. It was also found that the fabricated AgNP-BC is stable for more than 6 months.

BC as Reducing Agent for *in Situ* Synthesis of AuNPs. The procedure for *in situ* synthesis of AuNPs within BC was performed according to following method: Ten pieces of as-received wet BC (3 × 1 × 0.5 cm^3) were soaked in 100 mL of boiled solution of 50 mM $HAuCl_4$. Boiling was kept for 90 min under vigorous stirring. In this method, the penetrated gold ions into the BCs network are gradually reduced to AuNPs due to presence of hydroxyl groups on the surface of BCs which act as chemical reducing agent. The color change of BCs from colorless to pale purple confirms the synthesis of AuNPs. The fabricated AuNP-BC (*in situ* generated AuNPs in BC) were then separated from the reaction mixture and washed several times with double-distilled water in order to remove any free/weakly attached AuNPs or unreacted gold cations. The fabricated Au-BCs were kept in dark conditions at 4 °C before being used. The fabrication of Au-BCs was confirmed by UV−visible absorption spectra, EDX and SEM.

BC as a Nanonetwork Embedding AuNPs. Here, AuNP-BC was fabricated by modifying a previously reported method.[18] In brief, the as-received wet BC (15 × 10 × 0.5 cm^3) was soaked in 400 mL of boiled solution of 50 mM $HAuCl_4$ for 15 min followed by stirring. Afterward, 600 μL of 50% (v/v) PEI solution was rapidly injected into the reaction mixture and boiling was kept for 10 min. The fabricated Au-BCs were then separated from the reaction mixture and washed several times with double-distilled water in order to remove any free/weakly attached AuNPs or unreacted gold cations. In this method, the penetrated gold ions into the BC network are reduced to AuNPs by using PEI as a reducing agent. Here, BCs act as biotemplate for synthesis of AuNPs due to their porous scaffolds. The color change of BC from colorless to wine red endorses the presence of the AuNPs in the nanonetwork structure of BCs. The fabricated AuNP-BCs were kept in dark conditions at 4 °C before being used. The fabrication of AuNP-BC was confirmed by UV−visible absorption spectra, EDX and SEM.

Functionalization StrategyTto Embed the Photoluminescent Nanoparticles (PL-NPs) within Scaffolds of BC. To use BC as a template to embed the PL-NPs, there are two major steps that are needed to be performed: modification of BC *via* TEMPO-mediated oxidation to introduce carboxyl groups on its surface and then conversion of the carboxylated bacterial cellulose nanopaper (CBC) to amine-reactive by EDC/NHS activation in order to attach the PL-NPs to the functionalized BC.

Carboxylation of BC *via* TEMPO-Mediated Oxidation. Several methods have been proposed in order to obtain the carboxylation of cellulose. Among these methods, TEMPO-mediated oxidation is the most useful approach because of its numerous advantages compared to other methods.[37] TEMPO-mediated oxidation yields the selective oxidation of C6 primary hydroxyl groups of cellulose molecules and finally introduces the carboxyl group on the surface of BC nanofiber.[37] Here, carboxylated BC (CBC) was prepared *via* the TEMPO-mediated oxidation procedure.[37−39] Briefly, 15 pieces of BC (7.5 × 2.5 × 0.5 cm^3) were soaked in 100 mL of double-distilled water containing 3.3 mg of 2,2,6,6-tetramethylpiperidine-1-oxyl (TEMPO) and 33 mg of NaBr. The oxidation process was started by adding 150 μL of 12% aqueous NaOCl to the suspension mixture. The pH of the mixture was maintained constant at 10.5 ± 0.1 using 0.5 M NaOH solution under stirring at room temperature. After an additional 1 h of mixing, the oxidation was terminated by adding 2 mL of ethanol. The suspension was then neutralized to pH = 7 by 0.5 M HCl solution. The resulting carboxylated BC (CBC) was then washed several times with double-distilled water and ethanol.

Attachment of PL-NPs on CBC Using the EDC/NHS Coupling Chemistry. The PL-NPs can be covalently coupled to the carboxylic surface of the CBCs *via* EDC/NHS activation method. In a typical experiment, CBC was dipped in 10 mM acetate buffer solution with pH 4.5 for 30 min. The CBC was then transferred into 10 mM acetate buffer solution with pH 4.5 (background buffer) containing 0.1 M 1-ethyl-3-(3-(dimethylamino)propyl)carbodiimide (EDC) and 0.4 M *N*-hydroxysuccinimide (NHS) for 20 min at room temperature under stirring conditions. After that, the resultant amine activated CBC was rinsed several times using the acetate buffer solution (pH 4.5) in order to remove the excess of unreacted EDC and NHS from the films. The activated CBC was then utilized to covalently attach the PL-NPs such as streptavidin-conjugated QDs, amine-functionalized carbon dots, alkylamine-functionalized graphene oxide and upconversion nanoparticles. As a final step, the activated CBC were separately immersed in each solution of PL-NPs dispersion (pH 4.5) followed by stirring for 30 min. Thereafter, the PL-BC films were immersed in the 10 mM acetate buffer solution (pH 4.5) for 10 min, and then 10 mM carbonate buffer solution (pH = 8.5) and eventually several times rinsed with double-distilled water in order to remove any unbound and untreated PL-NPs from the BCs films. The PL-BCs films were stored in dark conditions at 4 °C before being used.

The procedure for rhodamine or trypan blue (or any compound with amino groups) attachment onto CBCs is similar to the procedure described above.

Sensing Platforms Fabrication. The wet fabricated nanopaper-based composites (NBCs) were dewatered by inserting them between two blotting papers which were sandwiched using two glass plates (6 mm in diameter) and spring-type binder clips. Afterward, the above setup was placed overnight in a 40 °C oven in order to dry the fabricated nopaper-based composites. The dried NBCs were then separated from the blotting papers.

As depicted in Supporting Information Figure S4, we exploited a wax printing machine to create the specific patterned layouts (two-dimensional cuvette and multiwell patterns) onto the dried films of the NBCs, forming hydrophobic barriers made of wax (the patterns were directly printed onto the NBC films). Initially, the desired patterns (cuvette and plate designs) were created in CorelDRAW X5 (Pantone, Inc., 2010) and then printed on normal paper. The dried NBCs were then attached on the printed patterns and then reprinted. Finally, after printing the wax onto the dried NBCs, they were separated from the paper. The printed NBC were stored in dark conditions at 4 °C before being used. Optionally, the NBCs dried films can be cut in circles using a hole punch device. The fabricated spots for individual assays made of NBCs can be placed into a microwell plate to be measured using a microplate reader, see Supporting Information Figure S4.

Using Spots for Individual Assays, Microtiter Plates and Cuvettes Made of BC. Two microliters (for microtiter plate and spot patterns) and 5 μL volumes (for cuvette design) of analytes solutions were separately dropped in their respective test zones. Since local refractive index may vary depending on wet conditions, the drop-casted solutions were dried for 30 min at room temperature.

GO as a Pathogen-Revealing Agent. Bacteria strains were obtained as previously reported.[36] QD-BC spots for individual assays were used across these experiments. The QD-BC spots were treated and measured in a black microwell plate as follows: Streptavidin-QD-BC spots were conjugated with biotinylated antibodies against *E. coli* (Ab) through streptavidin−biotin

interactions by drop casting 3 μL of antibodies concentrated at 400 μg mL^{-1} onto the studied QD-BC spots. Antibodies were diluted in phosphate-buffered saline (PBS) supplemented with Tween 20 at 0.5% (v/v) and bovine serum albumin at 1% (w/v). The Ab-QD-BC spots were incubated for 15 min and dried with a nitrogen stream. To remove the unbound Ab, the Ab-QD-BC spots were washed three times with 150 μL of PBS supplemented with Tween 20 at 0.05% (v/v) (PBST). The starting photoluminescent intesities were measured at this point. Then, the Ab-QD-BC spots were incubated with 100 μL of blank solutions and different suspensions of pathogens, including *E. coli* (at 10^3, 10^5 and 10^7 CFU mL^{-1}) and *S. typhimurium* (at 10^7 CFU mL^{-1}), for 30 min. PBS and tap water were used as matrix to perform this immunoassay. After that, the studied Ab-QD-BC spots were washed twice with 150 μL of PBST, twice with 150 μL of double-distilled water and incubated with 50 μL of GO concentrated at 90 μg mL^{-1} for 15 min. GO was dispersed in double-distilled water. Then, the Ab-QD-BC spots were washed twice with 150 μL of double-distilled water. Lastly, the microwells that contained the Ab-QD-BC spots were completely aspirated and their final photoluminescence was measured using the aforementioned spectrophotometer (microplate reader). The experiments were carried out in duplicate. The Ab-QD-BC spots were excited at 480 nm. The photoluminescent intensities were normalized according to the maximum intensity of the studied spectrum.

Colorimetric Analysis of AuNP Embedded within BC and Nitrocellulose. BC and nitrocellulose spots of ~6 mm were obtained using a hole punch. One microliter of [AuNPs] = 276 nM was drop-casted onto the respective spot. After that, the spots were dried at room temperature during 15 min. The concentration of the embedded nanoparticles was increased by repeating the steps before 5 times. The intensity of the optical signals was recorded on a white background using an ESEQuant lateral flow reader (Qiagen GmbH, Germany).

Using Individual Spots of BC as a Preconcentration Membrane. BC spots of 6 mm were obtained using a hole punch. The BC spots were put inside a microwell and were drop-casted with 4 μL of [AuNP] = 1.84 μM/[QDs] = 100 nM. The spectra of the AuNP/QDs embedded within the BC spot were obtained using the aforementioned spectrophotometer (microplate reader).

Synthesis of AuNP. AuNPs exhibiting an average diameter of 20 nm were synthesized using previously reported procedures.[40]

Conflict of Interest: The authors declare no competing financial interest.

Supporting Information Available: Figures S1−S15, Table S1 and details on synthesis and characterization of BC and UCNP. The Supporting Information is available free of charge on the ACS Publications website at DOI: 10.1021/acsnano.5b03097.

Acknowledgment. This work was supported by MINECO (Spain, MAT2014-52485-P, BIO2013-49464-EXP). ICN2 acknowledges support from the Severo Ochoa Program (MINECO, Grant SEV-2013-0295).

REFERENCES AND NOTES

1. Klemm, D.; Heublein, B.; Fink, H.-P.; Bohn, A. Cellulose: Fascinating Biopolymer and Sustainable Raw Material. *Angew. Chem., Int. Ed.* **2005**, *44*, 3358–3393.
2. Lynd, L. R.; Weimer, P. J.; van Zyl, W. H.; Pretorius, I. S. Microbial Cellulose Utilization: Fundamentals and Biotechnology. *Microbiol. Mol. Biol. Rev.* **2002**, *66*, 506–577.
3. Klemm, D.; Kramer, F.; Moritz, S.; Lindström, T.; Ankerfors, M.; Gray, D.; Dorris, A. Nanocelluloses: A New Family of Nature-Based Materials. *Angew. Chem., Int. Ed.* **2011**, *50*, 5438–5466.
4. Moon, R. J.; Martini, A.; Nairn, J.; Simonsen, J.; Youngblood, J. Cellulose Nanomaterials Review: Structure, Properties and Nanocomposites. *Chem. Soc. Rev.* **2011**, *40*, 3941–3994.
5. Wei, H.; Rodriguez, K.; Renneckar, S.; Vikesland, P. J. Environmental Science and Engineering Applications of Nanocellulose-Based Nanocomposites. *Environ. Sci.: Nano* **2014**, *1*, 302–316.
6. Nge, T.; Sugiyama, J. Biomimetic Mineralization of Apatite on Bacterial Cellulose. In *Bacterial NanoCellulose: A Sophisticated Multifunctional Material*; M. Gama, P., Gatenholm, D. K., Eds.; CRC Press: Boca Raton, FL, 2013; pp 217−238.
7. Phisalaphong, M.; Chiaoprakobkij, N. Applications and Products—Nata de Coco. In *Bacterial NanoCellulose: A Sophisticated Multifunctional Material*; Gama, M., Gatenholm, P., Klemm, D., Eds.; CRC Press: Boca Raton, FL, 2013; pp 143−156.
8. Czaja, W.; Krystynowicz, A.; Bielecki, S.; Brown, R. M., Jr. Microbial Cellulose—the Natural Power to Heal Wounds. *Biomaterials* **2006**, *27*, 145–151.
9. Lin, N.; Dufresne, A. Nanocellulose in Biomedicine: Current Status and Future Prospect. *Eur. Polym. J.* **2014**, *59*, 302–325.
10. Huang, J.; Zhu, H.; Chen, Y.; Preston, C.; Rohrbach, K.; Cumings, J.; Hu, L. Highly Transparent and Flexible Nanopaper Transistors. *ACS Nano* **2013**, *7*, 2106–2113.
11. Yan, C.; Wang, J.; Kang, W.; Cui, M.; Wang, X.; Foo, C. Y.; Chee, K. J.; Lee, P. S. Highly Stretchable Piezoresistive Graphene−Nanocellulose Nanopaper for Strain Sensors. *Adv. Mater.* **2014**, *26*, 2022–2027.
12. Svagan, A. J.; Busko, D.; Avlasevich, Y.; Glasser, G.; Baluschev, S.; Landfester, K. Photon Energy Upconverting Nanopaper: A Bioinspired Oxygen Protection Strategy. *ACS Nano* **2014**, *8*, 8198–8207.
13. Fang, Z.; Zhu, H.; Yuan, Y.; Ha, D.; Zhu, S.; Preston, C.; Chen, Q.; Li, Y.; Han, X.; Lee, S.; et al. Novel Nanostructured Paper with Ultrahigh Transparency and Ultrahigh Haze for Solar Cells. *Nano Lett.* **2014**, *14*, 765–773.
14. Zhu, H.; Jia, Z.; Chen, Y.; Weadock, N.; Wan, J.; Vaaland, O.; Han, X.; Li, T.; Hu, L. Tin Anode for Sodium-Ion Batteries Using Natural Wood Fiber as a Mechanical Buffer and Electrolyte Reservoir. *Nano Lett.* **2013**, *13*, 3093–3100.
15. Choi, K.-H.; Cho, S.-J.; Chun, S.-J.; Yoo, J. T.; Lee, C. K.; Kim, W.; Wu, Q.; Park, S.-B.; Choi, D.-H.; Lee, S.-Y.; et al. Heterolayered, One-Dimensional Nanobuilding Block Mat Batteries. *Nano Lett.* **2014**, *14*, 5677–5686.
16. Olsson, R. T.; Azizi Samir, M. A. S.; Salazar-Alvarez, G.; Belova, L.; Strom, V.; Berglund, A. L.; Ikkala, O.; Nogues, J.; Gedde, U. W. Making Flexible Magnetic Aerogels and Stiff Magnetic Nanopaper Using Cellulose Nanofibrils as Templates. *Nat. Nanotechnol.* **2010**, *5*, 584–588.
17. Korhonen, J. T.; Hiekkataipale, P.; Malm, J.; Karppinen, M.; Ikkala, O.; Ras, R. H. A. Inorganic Hollow Nanotube Aerogels by Atomic Layer Deposition onto Native Nanocellulose Templates. *ACS Nano* **2011**, *5*, 1967–1974.
18. Zhang, T.; Wang, W.; Zhang, D.; Zhang, X.; Ma, Y.; Zhou, Y.; Qi, L. Biotemplated Synthesis of Gold Nanoparticle−Bacteria Cellulose Nanofiber Nanocomposites and Their Application in Biosensing. *Adv. Funct. Mater.* **2010**, *20*, 1152–1160.
19. Zhang, B.; Zhou, J.; Li, S.; Zhang, X.; Huang, D.; He, Y.; Wang, M.; Yang, G.; Shen, Y. Hydrogen Peroxide Biosensor Based on Microperoxidase-11 Immobilized on Flexible MWCNTs-BC Nanocomposite Film. *Talanta* **2015**, *131*, 243–248.
20. Parolo, C.; Merkoci, A. Paper-Based Nanobiosensors for Diagnostics. *Chem. Soc. Rev.* **2013**, *42*, 450–457.
21. Walt, D. R. Miniature Analytical Methods for Medical Diagnostics. *Science* **2005**, *308*, 217–219.
22. Brown, A. J. XLIII.-On an Acetic Ferment Which Forms Cellulose. *J. Chem. Soc., Trans.* **1886**, *49*, 432–439.
23. Anker, J. N.; Hall, W. P.; Lyandres, O.; Shah, N. C.; Zhao, J.; Van Duyne, R. P. Biosensing with Plasmonic Nanosensors. *Nat. Mater.* **2008**, *7*, 442–453.
24. Howes, P. D.; Chandrawati, R.; Stevens, M. M. Colloidal Nanoparticles as Advanced Biological Sensors. *Science* **2014**, *346*, 1247390.
25. Naik, G. V.; Shalaev, V. M.; Boltasseva, A. Alternative Plasmonic Materials: Beyond Gold and Silver. *Adv. Mater.* **2013**, *25*, 3264–3294.
26. Biswas, N.; Thomas, S.; Sarkar, A.; Mukherjee, T.; Kapoor, S. Adsorption of Methimazole on Silver Nanoparticles: FTIR, Raman, and Surface-Enhanced Raman Scattering Study Aided by Density Functional Theory. *J. Phys. Chem. C* **2009**, *113*, 7091–7100.

27. Abbasi, S.; Khani, H.; Hosseinzadeh, L.; Safari, Z. Determination of Thiourea in Fruit Juice by a Kinetic Spectrophotometric Method. *J. Hazard. Mater.* **2010**, *174*, 257–262.
28. Wei, S.-C.; Hsu, P.-H.; Lee, Y.-F.; Lin, Y.-W.; Huang, C.-C. Selective Detection of Iodide and Cyanide Anions Using Gold-Nanoparticle-Based Fluorescent Probes. *ACS Appl. Mater. Interfaces* **2012**, *4*, 2652–2658.
29. Resch-Genger, U.; Grabolle, M.; Cavaliere-Jaricot, S.; Nitschke, R.; Nann, T. Quantum Dots *versus* Organic Dyes as Fluorescent Labels. *Nat. Methods* **2008**, *5*, 763–775.
30. Michalet, X.; Pinaud, F. F.; Bentolila, L. A.; Tsay, J. M.; Doose, S.; Li, J. J.; Sundaresan, G.; Wu, A. M.; Gambhir, S. S.; Weiss, S. Quantum Dots for Live Cells, *in Vivo* Imaging, and Diagnostics. *Science* **2005**, *307*, 538–544.
31. Medintz, I. L.; Uyeda, H. T.; Goldman, E. R.; Mattoussi, H. Quantum Dot Bioconjugates for Imaging, Labelling and Sensing. *Nat. Mater.* **2005**, *4*, 435–446.
32. Somers, R. C.; Bawendi, M. G.; Nocera, D. G. CdSe Nanocrystal Based Chem-/bio- Sensors. *Chem. Soc. Rev.* **2007**, *36*, 579–591.
33. Chen, G.; Qiu, H.; Prasad, P. N.; Chen, X. Upconversion Nanoparticles: Design, Nanochemistry, and Applications in Theranostics. *Chem. Rev.* **2014**, *114*, 5161–5214.
34. Loh, K. P.; Bao, Q.; Eda, G.; Chhowalla, M. Graphene Oxide as a Chemically Tunable Platform for Optical Applications. *Nat. Chem.* **2010**, *2*, 1015–1024.
35. Morales-Narváez, E.; Merkoçi, A. Graphene Oxide as an Optical Biosensing Platform. *Adv. Mater.* **2012**, *24*, 3298–3308.
36. Morales-Narváez, E.; Hassan, A.-R.; Merkoçi, A. Graphene Oxide as a Pathogen-Revealing Agent: Sensing with a Digital-Like Response. *Angew. Chem., Int. Ed.* **2013**, *52*, 13779–13783.
37. Ifuku, S.; Tsuji, M.; Morimoto, M.; Saimoto, H.; Yano, H. Synthesis of Silver Nanoparticles Templated by TEMPO-Mediated Oxidized Bacterial Cellulose Nanofibers. *Biomacromolecules* **2009**, *10*, 2714–2717.
38. Orelma, H.; Filpponen, I.; Johansson, L.-S.; Osterberg, M.; Rojas, O. J.; Laine, J. Surface Functionalized Nanofibrillar Cellulose (NFC) Film as a Platform for Immunoassays and Diagnostics. *Biointerphases* **2012**, *7*, 61.
39. Li, X.; Chen, S.; Hu, W.; Shi, S.; Shen, W.; Zhang, X.; Wang, H. *In Situ* Synthesis of CdS Nanoparticles on Bacterial Cellulose Nanofibers. *Carbohydr. Polym.* **2009**, *76*, 509–512.
40. Nunes Pauli, G. E.; de la Escosura-Muñiz, A.; Parolo, C.; Helmuth Bechtold, I.; Merkoçi, A. Lab-in-a-Syringe Using Gold Nanoparticles for Rapid Immunosensing of Protein Biomarkers. *Lab Chip* **2015**, *15*, 399–405.